Design Process for a Parallel LLC Resonant Converter for Powered Electric Vehicle Charging Systems

Borislav Dimitrov[1], Andrew Cruden[2], Suleiman Sharkh[3], Carlos Ponce-de-Leon[4], Tom Bryden[5], George Hilton[6]

University of Southampton, Engineering Science, Southampton, UK

Abstract: *In this paper a design procedure of parallel-connected LLC converters for PV powered car battery charging is presented. Matching the characteristics of the converters and the PV generator is shown to be critical to achieving efficient conversion. Experimental results are presented to demonstrate the efficiency of the proposed design procedure. The aim of this research is to investigate the design procedure for matching between the parameters of the converters and the photovoltaic generator.*

Keywords: LLC resonant converter, PV system, design, electrical vehicle

1. Introduction

The proposed system for electric vehicle battery charging is based on a photovoltaic (PV) generator, backup battery and two DC/DC converters as shown in Fig.1. All converters and sources are separate with individual switches. The system works in the following modes: renewable energy harvesting to charge the backup battery during the day; charging the electric vehicle battery during the night using energy from the backup battery or alternatively from the public grid if the accumulated energy is not enough; car battery charging directly from photovoltaic system during the day.

This paper presents the design procedure and experimental results of the second DC/DC converter, which is accomplished from six LLC half-bridge resonance converters in parallel as shown in Fig.2. In this research the converters are powered directly from the PV generator, the design of which is also shown.

The proposed system is flexible and allows for future upgrade. Larger installed power for powerful batteries or faster charge is achievable with adding more modules and converters.

Resonant LLC converters have been the object of wide research [1,2,3,4] due to their significant advantages: high efficiency; soft switching on the first side, achievable with zero voltage switching (ZVS); soft switching on the second side, achievable with zero current switching (ZCS); ability of line and load regulation. Some publications are focused on battery charging and parallel operation of the converters [1,2,3] and many reports present their precise design procedures [5,6,7].

The use of the LLC converters in parallel, powered by a PV generator is presented. Several assumptions are made:
- Although the converter takes energy from a backup battery or electrical grid, in some conditions it is possible to be powered from the PV generator via a DC/DC converter. In this case, the input power can vary over large ranges, which requires the line regulation to be considered on the design level.
- In the nominal condition all converters in parallel must work with point gain equal to one ($G=$), which requires equality between switching F and resonance frequency.
- The converters have to adhere to all mandatory for LLC topology requirements: work with ZVS in the inductive region on a gain-normal frequency diagram; work in the vicinity of the point $G=$; work on the maximum efficiency for these class of converters, which is around 95%.

The aim of this research is to investigate the design procedure for matching between the parameters of the converters and the photovoltaic generator. This requires design of the converter with a relatively wide input voltage range (for example in range of 300V), compared with a conventional grid connected system (in range of 60V). The input voltage depends on solar energy variation as well as ambient and surface temperature of the modules, and because of this the design procedure of the PV generator is also presented.
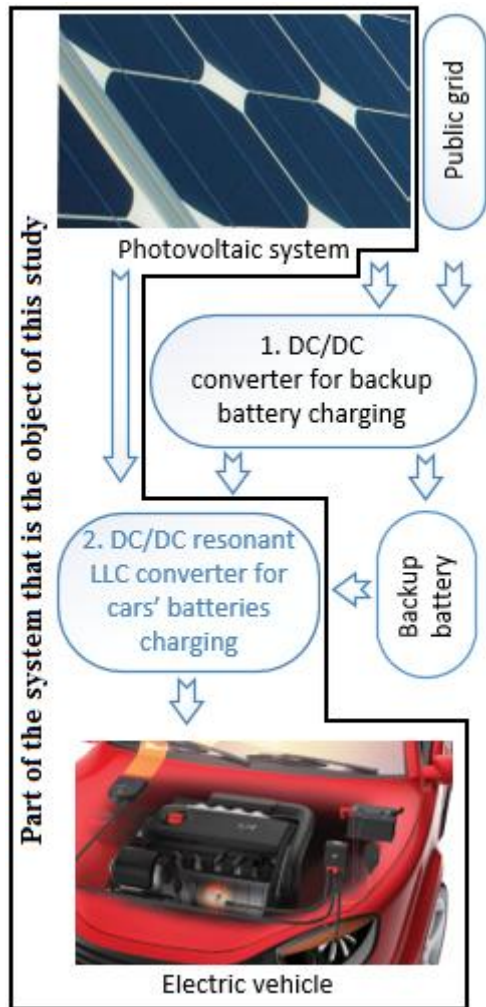
Figure 1: Block diagram of the entire system for battery charging
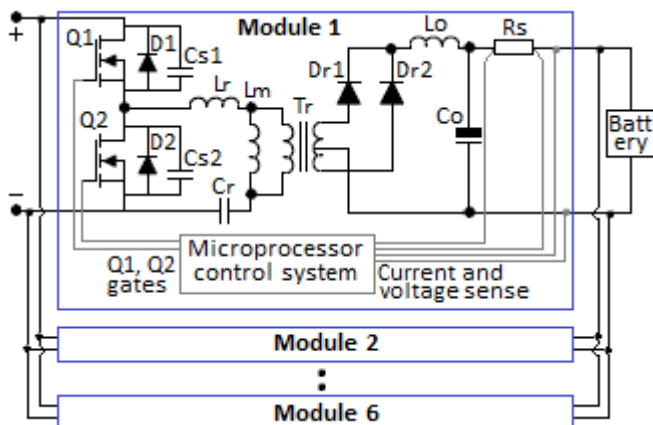

Figure 2: LLC converters for electrical vehicle charging in parallel

The schematics from Fig.2 uses the following elements: Q1, Q2 – MOSFET transistors used for half bridge, with reverse diodes D1, D2 and Cs1, Cs2 Drain-Source junction capacitors; Lr, Cr – resonance inductance and capacitor; Lm – magnetic inductance; Tr – transformer; Dr1, Dr2 – second side rectifier; Lo, Co – second side filter; Rs – current sense resistor.

2. Design of the resonant LLC converter

The design procedure, based on first harmonic analysis [7,8], is applied for the six converters in parallel. The substitute circuit is shown in Fig. 3, where   is resonant capacitor;   in magnetizing inductance;   is parasitic capacitance on the first side of the transformer and the PCB layout;   is reflected load resistance.
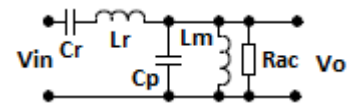

Figure 3: Substitute resonance circuit.

The basic equations describing the design procedure are [5,6,7,9]:

$$G(Q, m, F_x) = \left| \frac{V_o}{V_{in}} \right| = $$
$$= \frac{F_x^2 (m - 1)}{\sqrt{(m.F_x^2 - 1)^2 + F_x^2.(F_x^2 - 1)^2.(m - 1)^2.Q^2}} \qquad (1)$$

where: G is the gain;

$$Q = \frac{\sqrt{L_r}}{R_a} \qquad (2)$$

is the quality factor;

$$F_x = \frac{F}{} \qquad (3)$$

is the normalized frequency;

$$m = \frac{L_r +}{L_1} \qquad (4)$$

is ratio of the total primary inductance to the resonant inductance.

The reflected load resistance is:

$$R_{ac} = \frac{8}{\pi^2} . \frac{N_{pri}^2}{N_{sec}^2} . \qquad (5)$$

where   is output load.

The resonant capacitor   and resonance inductance   are calculated respectively as:

$$C_r = \frac{1}{2.\pi.Q.F_r.} \qquad (6)$$

$$L_r = \frac{1}{(2.\pi.F_r)^2} \qquad (7)$$

The parasitic capacitor is usually not present in the substitution circuit in established design procedure. InFig.3, represents the sum of the parasitic drain-source capacitance C and parasitic capacitance of the transformer's first side. In order to describe the minimum dead time   should not be neglected as a parameter, especially when high voltage, high power MOSFET transistors are used.

Equation (1) including   can be written as:

$$G(j\omega) = \frac{V_{out}}{V_{in}} \qquad (8)$$

where $\omega = 2.$

$$G(j\omega)=\cfrac{\cfrac{1}{\frac{1}{R_{ac}}+\frac{1}{j\omega L_m}+j\omega C_p}}{\frac{1}{j\omega\,C_r}+j\omega\,m+\cfrac{1}{\frac{1}{R_{ac}}+\frac{1}{s\,L_m}+j\omega}} \qquad (9)$$

Eventually, the network gain can be expressed as:

$$G(j\omega)=\cfrac{j\omega^2}{j\omega^4\frac{mC_p}{m}+j\omega^3\frac{L_g}{m\,R}} \qquad (10)$$
$$+j\omega^2\left(\frac{C_p L_m k_r^2}{m}+\frac{1}{m}\right)$$
$$+j\omega\,\frac{L_m k_r^2}{m R_{ac}}+\frac{k_r^2}{m}$$

where $\quad k_r = 1/\sqrt{L_r}.$

The condition to achieve ZVS is achieved if the expression below is met, which is dependent on the inductances and the parasitic capacitance:

$$\frac{(L_m+L_r)\cdot I_{mpk}^2}{2} \geq \frac{(2\cdot C_p)\cdot}{2} \qquad (11)$$
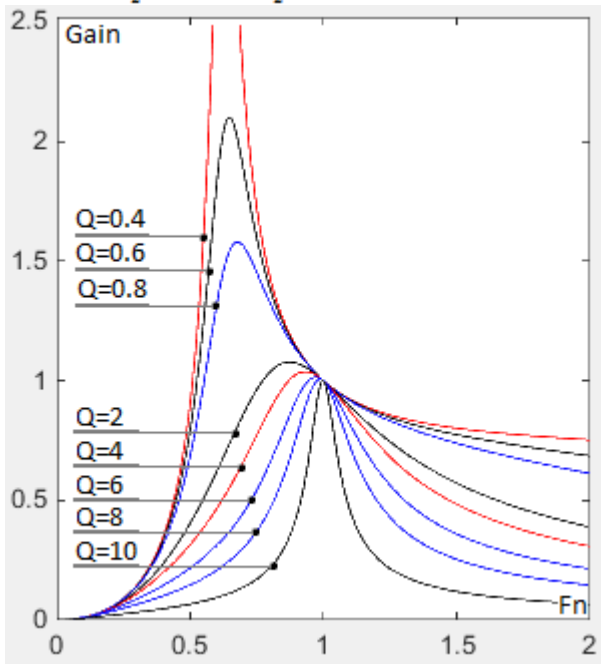

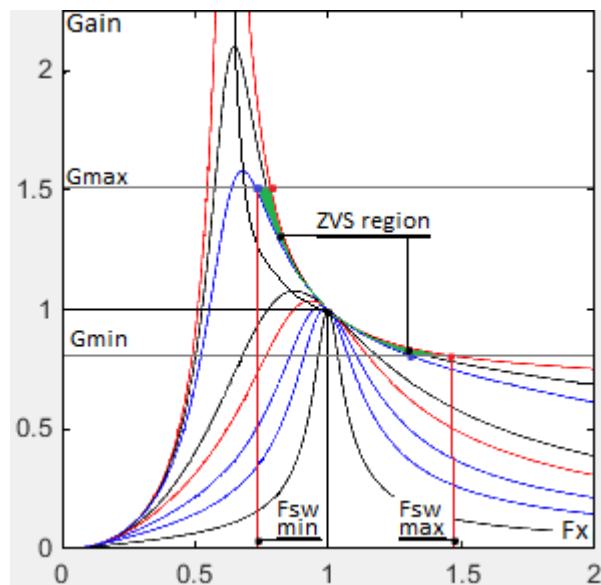**Figure 4:** Gain – normal frequency dependency

Figure 5: Quality factor, normalized switching frequency range and zero voltage switching (ZVS) regions.

The minimum $(V_{in\,min})$ and maximum $(V_{in\,max})$ input voltages depend on the photovoltaic generator's characteristics and input power. In design, the input voltage range is determined by minimum (G_{min}) and maximum (G_{max}) gain respectively:

$$G_{min} = \frac{n\cdot(V_{out\,min}+V_f)}{V_{in\,max}/2} \qquad (12)$$

$$G_{max} = \frac{n\cdot(V_{out\,max}+V_f)}{V_{in\,min}/2} \qquad (13)$$

Where V_f is voltage drop over the diodes Dr1 and Dr2; n is the turn ratio.

The following are characteristics of the design converter:
- Input voltages (from the photovoltaic generator): $V_{inmin} = 30$; $V_{innom} = 45$; $V_{inmax} = 55$.
- Rated output power: 1500 W.
- Output voltages: $V_{outmin} = 11$; $V_{outnom} = 12$; $V_{outmax} = 12$.
- Efficiency: 0.92 as first assumption; gradually will be improved to maximum efficiency of 0.95.
- Nominal output current: $I_{nomout} = 12.$
- Switching frequency: $F_{sw} = 100kH$

The quality factor (eq. 2) and inductance ratio are chosen from a Matlab script, specialized for design of the resonance network of the converter. Flowchart1 shows the necessary calculation procedure for determining the dependency between Gain and normalized frequency Fx (Fig.4 and Fig.5).

Flowchart1.

```
clear
global Gain1; Gain1 =[];
                        % Matrices for the gain
global Gain25 ; Gain25 = [];
Q = [0.1, 0.2, ……, 10 ];    % Quality factor

fn = 0:0.01:2 ;            % 200 values for the
                          % normalized frequency
                          % according eq. 3. Value 100 is
                          % Fx=1 and value 200 is Fx=2

for m = 2:12        % ratio of total primary
                    % inductance to resonant
                    % inductance between 2 and 12
for i=1:201         % calculation of the Gain according to
                    % eq. 1
Gain1 (i) =  (fn(i)^2*(m-1)) / ( sqrt( (m*fn(i)^2-
1)^2+fn(i)^2*(fn(i)^2-1)^2*(m-1)^2*Q(1)^2 )) ;
                          % 25 or necessary graphics
Gain25
end
plot(fn, Gain1,'-r' … Gain25,'-r')  % plot the graphics for
                                    % the current m
i = 0 ;
pause ;
end
```

Fig.4 shows the curve of the Gain (eq. 1, 8, 9), calculated with constant inductance ratio (eq. 4), as function of normalized frequency (eq. 3).

In this design the inductance ratio is chosen: L_n = 3.5 and Q = 0.8, according to minimum and maximum gains.

The input voltage tolerance defined minimum (eq. 12) and maximum (eq. 13) gains as 0.78 and 1.51. In this case the working ZVS region and frequency range are shown on fig.5 as follows: minimum switching frequency $F_{swmin} = 75 kHz$; maximum switching frequency $F_{swmax} = 145 kHz$; resonance frequency $F_{sw} = F_{res} = 100 kHz$.

According eq. 5 the load at the nominal condition is $R_{ac} = 27.4\,\Omega$ and the load at 110% overload is $R_{ac} = 24.9\,\Omega$.

The resonance network has the follows parameters: resonance capacitance $C_r = 72.6\ nF$ (combined from three capacitors: 18nF, 22nF and 33nF in parallel), resonance inductance $L_r = 35\ \mu H$ and magnetic inductance $L_m = 136\ \mu H$. With these values the currents of the first and second side can be calculated.

The primary side RMS load current with 110% overload is 7.4 A, determined by the following equation:

$$I_{primRMS} = \frac{\pi}{2.\sqrt{2}} . \frac{I_{out}}{n} \qquad (14)$$

The magnetizing current at resonant frequency (100kHz) is 2.4 A and at minimal frequency is 3.2 A, determined by the following equation:

$$I_m = 0.901 \frac{n.V_{out}}{\omega.L_m} = 0.901 \frac{n.V_{out}}{2.\pi.F_{sw}.L_m} \qquad (15)$$

The resonant circuit current is 8.7A, determined by the following equation:

$$I_r = \sqrt{I_m^2 + I_{primRMS}^2} \qquad (16)$$

The total secondary side RMS current, determined from the primary side current, is 15.3 A.

$$I_{secRMS} = n.I_{primRMS} \qquad (17)$$

The secondary current is equally split into two transformer windings on the secondary side and amounts to 10.8A, calculated by:

$$I_{sw} = \frac{\sqrt{2}.I_{secRMS}}{2}, \qquad (18)$$

and the corresponding half-wave average current, according to the assumed circuit in fig.2, is 6.8 A calculated by:

$$I_{half-wave} = \frac{\sqrt{2}.I_{secRMS}}{\pi} \qquad (19)$$

According to the above calculations, the first side transistors are chosen as type IXFH14N80 [10]. The parasitic capacitance is $C_{ds} = 240\ pF$. Zero voltage switching is achievable according to expression 11, which has to be checked in the worst conditions. In this case, the energy accumulated in resonance and magnetizing inductance with maximum frequency and minimal magnetizing current is

228.8 μJ. The energy accumulated in parasitic capacitors in both transistors is 75.6 μJ. This means that the condition in expression 11 is met and ZVS in inductive region on fig.5 is achievable. The snubber capacitors Cs1 and Cs2 (fig.2) can use the standard value of 82pF.

The dead time at maximum frequency must be equal or higher than 0.0798 μs, according to:

$$t_{dead} \geq 16.C_p.F_{sw}.L_m \qquad (20)$$

3. Design of the Photovoltaic Generator

The experimental photovoltaic generator is built as a stand-alone system, used for powering the designed converters for battery charging. It is designed to match input characteristics of the converters and it has the follows characteristics: installed nominal power 15kW; voltage range: $V_{min} = 300V$, $V_{nom(STC)} = 450V$, $V_{maxOC} = 550V$; photovoltaic modules model APL200-18 with nominal power 200Wp at standard test conditions (STC); output current at the maximum power point of 47A; short circuit current of 52.3A. The generator schematic and its connection to the converters seen in Fig.1 are shown on Fig.6. The same figure shows the common parameters between the PV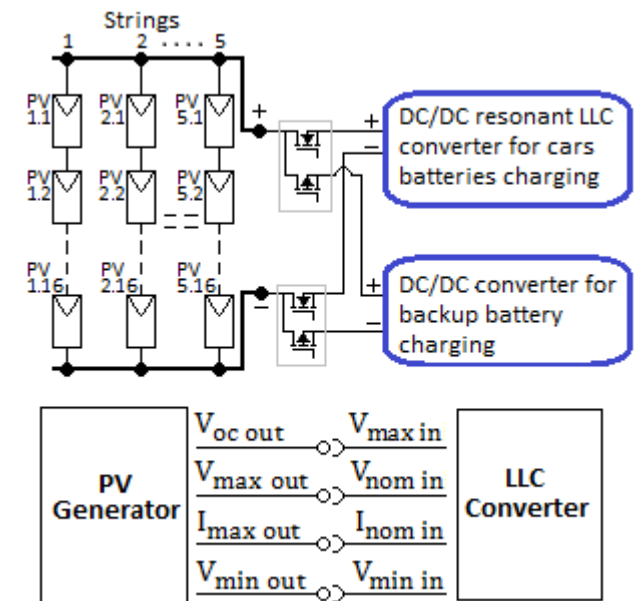 generator and the DC/DC LLC converter. The generator has 80 modules, connected as 5 strings in parallel with each string having 16 modules in series.

Figure 6: Schematic of the photovoltaic generator and the common parameters between the generator and the DC/DC LLC converter.

The design procedure of the photovoltaic generator is based on basic equations, which represent voltage and current tolerances as temperature dependent [11,12,13]. The minimum and maximum output voltages from a module are:

$$V_{min} = V_{mpp (stc)} + T_{KV}.\Delta\tau_{max} = 24.13V \qquad (21)$$

where: $\Delta\tau_{max}$ is the temperature difference between the maximum temperature and the temperature at STC: $\Delta\tau_{max} = 70^o - 25^oC$, $V_{mpp(stc)} = 26.1V$ is the output

voltage of one module at the maximum power point, and $T_{KV} = -0.0437V/C^o$ is the voltage temperature coefficient.

With this, the minimum voltage from 16 modules in series is 386V, which will be the minimum voltage for the converter, or the assumed above 300V meets this parameter.

$$V_{max} = V_{mpp(stc)} + T_{KV}.\Delta\tau_{min} = 27.85V \qquad (22)$$

where: $\Delta\tau_{mim}$ is the temperature difference between the minimum ambient temperature and the temperature at the standard test condition: $\Delta\tau_{min} = -15^o$ to $+25^oC$.

The maximum voltage is 445.6V which corresponds to nominal voltage of the converter, assumed as 450V.

The maximum output voltage on open circuit (OC) is calculated according to:

$$V_{OC} = V_{OC(stc)} + T_{KV}.\Delta\tau_{min} = 33.94V \qquad (23)$$

Maximum voltage on open circuit of the PV generator is 543.4V. This corresponds to assumed maximum voltage of the converter of 550V and would be working input voltage at light load.

The minimum and maximum current depend on the temperature coefficient $T_{KI} = 0.0038A/C^o$, are calculated as:

$$I_{min} = I_{mpp(stc)} + T_{KI}.\Delta\tau_{min} = 7.499A \qquad (24)$$
$$I_{max} = I_{mpp(stc)} + T_{KI}.\Delta\tau_{max} = 7.841A \qquad (25)$$

Where: $I_{mpp(stc)} = 7.67A$ is the current at the standard test condition.

With this the minimum power from 5 strings in parallel is:

$$P_{min} = 5.I_{min}.V_{min} = 14.5kW \qquad (26)$$

The maximum power is:

$$P_{max} = 5.I_{max}.V_{max} = 17.5kW \qquad (27)$$

The nominal power responding to standard test condition is:

$$P_{nom} = 5.I_{mpp(stc)}.V_{mpp(stc)} = 16.014kW \qquad (28)$$

The parameters of the photovoltaic generator, according to assumed schematic on Fig.6, are shown on Fig.7 – output Volt-Ampere and Fig.8 – output Power-Volt characteristics. The maximum power points are shown as a function of received radiation. With this design, the radiation during the noon hours is typically between $600 - 800W/m^2$ and it produces output power between 8.8-11.9kW, which corresponds to installed power of the six resonant converters in parallel of 9kW installed power. This mean that the designed converter has enough input power.
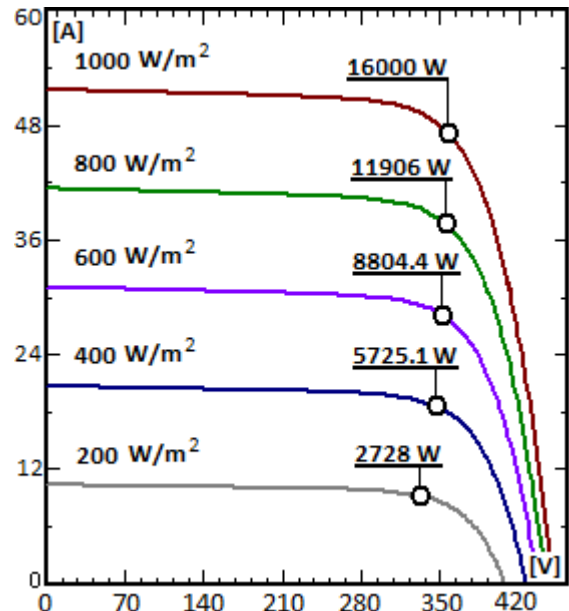

Figure 7: Output A-V characteristics of the photovoltaic generator.

With the assumed voltage region the system can even work with small radiation, around $50W/m^2$ (during the first or last hours of the day or worst whether conditions), producing 750W output power. With less power from the generator fewer converters should be operated in order to hold their high efficiency.
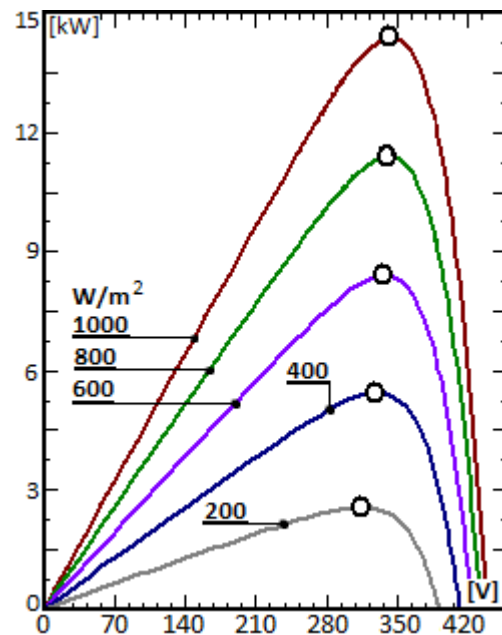

Figure 8: Output P-V characteristics of the photovoltaic generator

4. Experimental Results

An experimental charger was built and tested with several different batteries and converters in parallel, powered by a photovoltaic generator. The following figures show oscillograms of the converters:

- Fig.9.: Zero voltage switching of the resonant LLC converter. Curves 1 and 2 show gate drive signals. They

have equal values, although the oscillogram shows different voltages because of the differences between voltage and differential probes. Curve 3 is voltage over the resonant network, which crosses the zero point in the moment of the switching. Curve 4 is output DC voltage.

- Fig.10.: Characteristics of the converter, working under regulation with switching frequency smaller than resonant frequency: 1, 2 – gate drive signals; 3 – middle point voltage, which shows ZVS; 4 voltage over the resonant network.
- Fig. 11.: Output voltage (1) and current (2) of the converter, working under nominal load.
- Fig. 12.: Functional dependency between the efficiency of the converter and output power. Although the first assumption is 92% efficiency, after several calculations the maximum efficiency of 95% is achieved.
- Fig. 13.: Output voltage (1) and currents (2, 3, 4) on three converters in parallel. Output currents fluctuations depend on the output filter and in this design, they are around 20%.
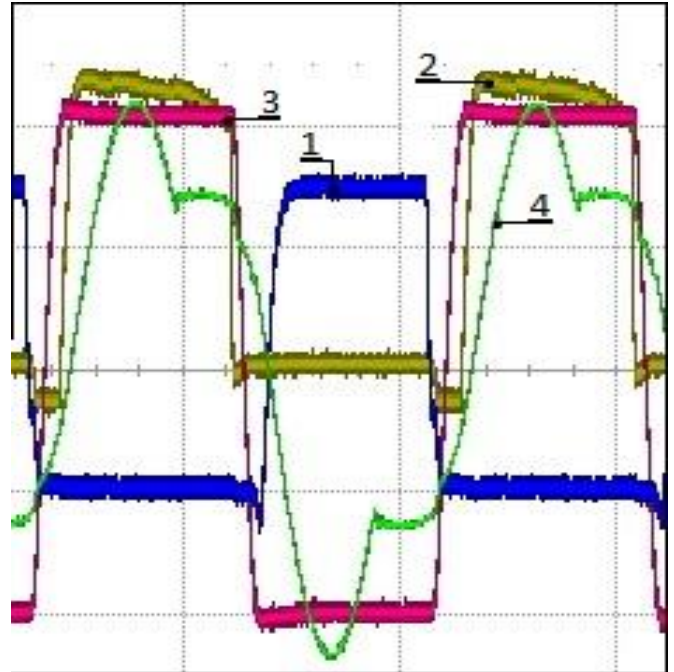

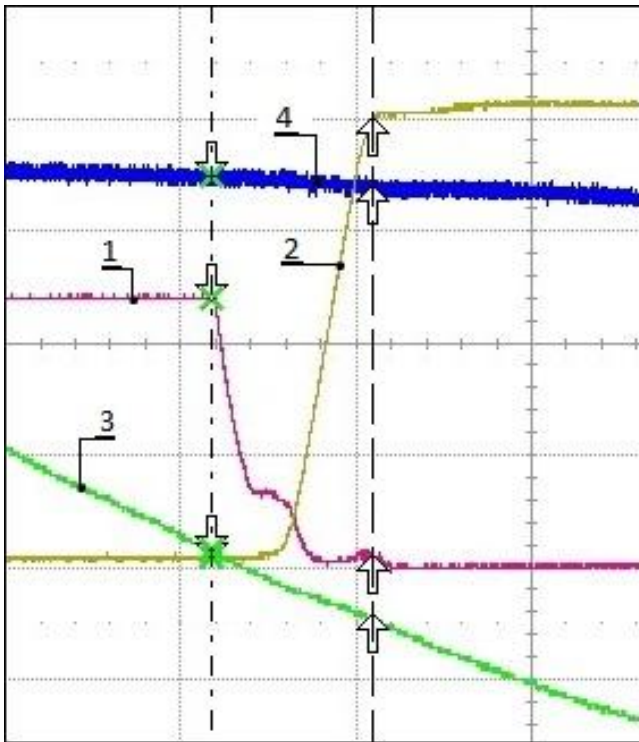**Figure 10:** Characteristics of the converter. Working frequency: 100kHz; 5 µs/div

Figure 11: Output voltage and current of the converter

Figure 12: Efficiency of the converter

Figure 9: Zero voltage switching of the resonant LLC converter. Working frequency: 100kHz; 5 µs/div

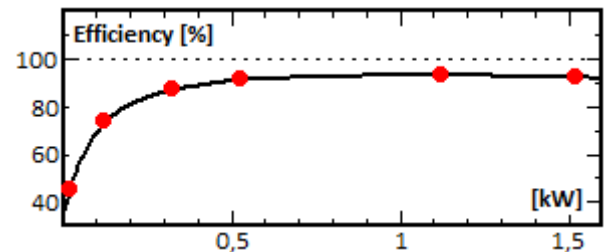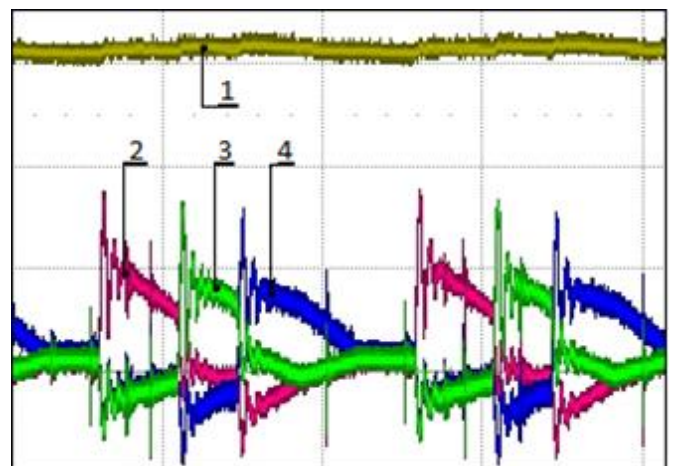**Figure 13:** Output voltage and currents.

5. Conclusion

The proposed system works as battery charging for electrical vehicle, using renewable energy from a photovoltaic generator. The following conclusions can be made:

- Design procedure of the LLC converter, based on first harmonic approximation is applicable for the investigated stipulated condition: converters in parallel, working in wide voltage range from a photovoltaic generator.
- Under this condition the converter can be designed to work in the ZVS region and normal for LLC converters efficiency. This is experimentally proved.
- The proposed system is robust, as failure of one of the converters does not stop the entire system.

This investigation is focused on a part of the entire system shown on fig.1. That suggests wide future research on this direction.

Acknowledge

References

[1] Christen D., S. Tschannen, J. Biela, Highly Efficient and Compact DC-DC Converter for Ultra-Fast Charging of Electric Vehicles, 15th International Power Electronics and Motion Control ConferenceECCE Europe, EPE-PEMC 2012

[2] Deng Junjun, Siqi Li, Sideng Hu, Chunting Chris Mi, Ruiqing Ma, Design Methodology of LLC Resonant Converters for Electric Vehicle Battery Chargers; IEEE Transactions On Vehicular Technology, VOL. 63, NO. 4, May 2014, p. 1581-1581

[3] Figge H., T. Grote, N. Froehleke, J. Boecker. Paralleling Of LLC Resonant Converters Using Frequency Controlled Current Balancing. IEEE Power Electronics Specialists Conference, 2008

[4] Gautam D., F. Musavi, M. Edington, W. Eberle, W. Dunford. An Automotive On-Board 3.3 kW Battery Charger for PHEV Application. IEEE Transactions on Vehicular Technology, Volume:61 ,Issue: 8, 2012

[5] Infineon. Design Guide for LLC Converter 2011. https://www.infineon.com/ (actual on 16/03/2017)

[6] Infineon. Resonant LLC Converter: Operation and Design. 2012 https://www.infineon.com/ (actual on 16/03/2017)

[7] Texas Instruments Incorporated. Designing an LLC Resonant Half-Bridge Power Converter 2011 https://www.ti.com/(actual on 16/03/2017)

[8] Nishimura T., Y. Adachi, Y. Ohta, K. Higuchi, E. Takegami, S. Tomioka, K. Jirasereeamornkul, K. Chamnongthai, Robust Digital Control for an LLC Current-Resonant DC-DC Converter, Ecti transactions on computer and information technology vol.7, NO.1 May 2013

[9] Monolithic Power Systems MPS. LLC Resonant Converter Using Resonant Controller HR1000, 2011 https://www.monolithicpower.com/ (actual on 16/03/2017)

[10] IXYS datasheet. Power MOSFET transistor IXFH14N80. 2002 http://www.ixys.com/(actual on 16/03/2017)

[11] German Energy Society, Planing and Instaling Photovoltaic Systems. Berlin 2008. ISBN-13:978-1-84407-442-6

[12] Rekuoua D, Matagne E, Optimization of Photovoltaic Power System. Modelization, Simulation and Control. Springer 2012. ISBN 978-1-4471-2348-4

[13] http://www.pvsyst.com/en/

Author Profile

Borislav Dimitrov received the M.E and PhD degrees in Electrical Engineering from Technical University of Varna in 2000 and 2008, respectively. Currently he is working as a researcher at the University of Southampton UK.

Andrew Crudenreceived the B.Eng. degree in electronic and electrical engineering, the M.Sc. degree in electrical power engineering, and the Ph.D. degree in the field of optical current sensing from the University of Strathclyde, Glasgow, U.K. In 2012 he became the Professor of Energy Technology at the University of Southampton, and is the Co-Director of the EPSRC CDT in Energy Storage and its Applications (www.energystorage-cdt.ac.uk).

Suleiman M. Sharkh received the B.Eng. and Ph.D.degrees in electrical engineering from the University of Southampton, Southampton, U.K., in 1990 and 1994, respectively. He is Professor of Power Electronics, Machines and Drives, and Head of the Mechatronics Research Group at the University of Southampton. He is also the Managing Director of HiT Systems Ltd. He has published over 160 papers in academic journals and conferences. His main research interests are in the area of control, electrical machine and power electronics with applications to electric vehicles, marine propulsion, exhaust energy recovery and submersible pumps. Prof. Sharkh is a senior member of the IEEE, a member of the IET and a Chartered Engineer. He was the 2008 winner of The Engineer Energy Innovation Award for his work on rim driven thrusters and marine turbine generators.

Carlos Ponce-de-Leon has a PhD in electrochemical engineering and works on redox flow batteries for energy storage, metal-air batteries, H_2/O_2, and borohydride fuel cells, metal ion removal, oxidation of organic compounds in wastewater, nanoelectro deposition. Involved in projects with the EPSRC and FP7.

Thomas Bryden received a MEng degree in Mechanical Engineering from the University of Warwick in 2007. Currently he is working as a PhD student at the University of Southampton UK.

George Hilton received his Frist Class MEng Degree in Mechanical Engineering with Advanced Materials from the University of Southampton in 2014. He then went on to join the CDT Energy Storage and its Applications to complete his PhD.